Composite Structures 303 (2023) 116369

Contents lists available at ScienceDirect

Composite Structures

journal homepage: www.elsevier.com/locate/compstruct

An innovative frictional anchorage system for flat CFRP ribbon strips

Viktor Gribniak [a,b,*], Aleksandr K. Arnautov [c], Arvydas Rimkus [a,b]

[a] Laboratory of Innovative Building Structures, Vilnius Gediminas Technical University, Vilnius, Lithuania
[b] Department of Steel and Composite Structures, Vilnius Gediminas Technical University, Vilnius, Lithuania
[c] Institute for Mechanics of Materials, University of Latvia, Riga, Latvia

ARTICLE INFO

Keywords:
CFRP strip
Spiral anchorage
Friction
Analytical model
3D-printing
Mechanical tests

ABSTRACT

Unidirectional carbon fibre-reinforced polymer (CFRP) materials represent a promising alternative to steel because of their lightweight, high tensile strength, and excellent corrosion and fatigue resistance. Stress-ribbon structural systems define the potential application object of unidirectional flat CFRP strips. However, anchorage difficulties make this idea problematic—the typical gripping systems are inefficient for anchoring the CFRP ribbons because of the tremendous thrust forces-induced stress concentration. Thus, the innovative frictional spiral anchorage system of the flat CFRP strips is the object of this study, which formulates the design principles for the frictional joins. Furthermore, the proposed theoretical model minimises the gripping system size, satisfying the CFRP strength limitation when the developed modified Archimedean spiral determines the shape of the contact surface. This work experimentally demonstrates the theoretical concept's adequacy—the mechanical resistance prediction error does not exceed 7% in the loading range covering the service load conditions. In addition, the manuscript presents several examples of frictional gripping systems, including the stress-ribbon pedestrian bridge prototype, and provides further insights into the frictional anchorage systems.

1. Introduction

The need to develop materials with mechanical properties tailored for construction has resulted from the current industrial trends [1]. Unidirectional carbon fibre-reinforced polymer (CFRP) materials represent a promising alternative to steel because of their lightweight, high tensile strength, and excellent corrosion and fatigue resistance [2–4]. Stress-ribbon structural systems allow applying the unidirectional flat CFRP strips. These systems are efficient for pedestrian bridges and long-span roofs [4,5]. However, tremendous thrust forces acting on the ribbons and the CFRP materials' vulnerability to the stress concentration in the clamped region raise the anchorage problems [5–7], and the typical gripping systems are inefficient for this purpose, causing the stress concentration in the ribbon [8,9]. Furthermore, the CFRP shear resistance and compressive strength are only about 1/10–1/20 of the longitudinal tensile strength [10]. Therefore, reducing the peak clamping stresses determines the current research interest [9,11,12].

The first bridge prototype with CFRP ribbons was constructed in Germany in 2007 [13]. The non-laminated strip-loop cables formed the load-bearing component of the bridge system, conforming to the terminology [14]. Meier and Winstoerfer patented this close-loop ribbon concept in 2001 [15] when unidirectional continuous CFRP (thermoplastic) tapes layer-by-layer wound around the pins at the supports. As a result, this cable system has a uniform strain distribution. Furthermore, the disintegrated structure of the wound layers reduces the bending stress concentration on the supports, which could dramatically increase with the thickness increase in the laminated strips [5]. At the same time, the non-integrity of the ribbon structure makes it highly vulnerable to the failure of any CFRP layer because of the continuous wound layout, representing a single long strip, and the absence of adhesive contact between the layers, which could prevent the loops from being released.

The authors proposed a frictional spiral anchorage system [16] to overcome the stress concentration problem and preserve the structural integrity of the flat CFRP strip. Following the proposed scheme, the contact surface curvature equals zero at the strip entering point and gradually increases in the anchorage device, as Fig. 1**a** shows. The internal clamps fix the CFRP strip at an early loading stage until the main spiral grips activate the frictional shear stresses, reducing the axial load gradually over the spiral length. Thus, the internal grips do not face significant tensioning; the resultant tensile stresses in the strip due to the

* Corresponding author at: Head of Laboratory of Innovative Building Structures and Professor of Department of Steel and Composite Structures, Vilnius Gediminas Technical University, Sauletekio av. 11, Vilnius LT-10223, Lithuania.
E-mail address: Viktor.Gribniak@vilniustech.lt (V. Gribniak).

https://doi.org/10.1016/j.compstruct.2022.116369
Received 28 April 2022; Received in revised form 21 September 2022; Accepted 11 October 2022
Available online 17 October 2022

tension and bending loads' combined effect do not exceed the tensile strength because of the balance between the curvature increase of the spiral support and steadily decreasing the tension force. The ratio between the external load and the internal clamps' reaction, i.e., the traction coefficient, describes the anchorage effect. This coefficient determines the design parameter, and the study [16] verified the corresponding analytical model by testing the anchorage prototype with the polymeric grips. However, the development of an efficient geometry of the spiral grips remained beyond the scope of the previous work.

This study develops the anchorage prototype optimising the geometry for compact spiral distribution to ensure the gripping system's specific traction ratio. The modified Archimedean spiral determines the optimised solution, which is the experimental verification object of this research.

2. Theoretical concept

2.1. The current state of knowledge

Unidirectional FRPs are vulnerable to loads misaligned with the fibre orientation. For instance, the 1° load deviation reduced the FRP resistance by 30% [17]. The end-tab bonding can solve this problem, but the faulty installation can cause premature failure of the FRP samples [6], with the tab material's rigidity affecting the ultimate resistance [18]. Furthermore, the friction-induced shear stress distribution is not uniform, with the peak localised at the contact boundary edge [11,18–20]. The above mechanisms concentrate the strip stress inside the anchorage devices, causing a premature failure of the FRP component [16].

Pagano et al. [21] experimentally related the reliability of the tab connection with reducing the stress peak, moving it inward the gripping device. Eliasson et al. [22] applied the stress shifting scheme to improve the anchorage device's fatigue resistance. The latter feature is vital for structural stress-ribbon systems continuously facing dynamic and cyclic loads [7]. Unfortunately, the developed anchorage systems are feasible for laboratory tests only.

Furthermore, the frictional systems cannot remove the stress peak, smoothing it over the contact zone. Moreover, the stress distribution shape, in essence, does not change, i.e. the stresses from the maximum value appearing at the entry of the gripping device decrease throughout the contact surface [16]. Portnov et al. [8] developed the variable curvature anchorage concept to control the friction-induced stresses over the contact surface. Unfortunately, the experimental implementation of this idea was not successful—the failure of the CFRP strip inside the grips indicated the systems' inability to smooth the contact stresses efficiently.

The study [16] presented the evolutionary development of the frictional device capable of anchoring a high-strength unidirectional CFRP strip when the logarithmic spiral describes the contact surface geometry. This study extends the developed analytical model for optimising the anchorage prototype size essential for engineering applications.

2.2. The research idea

The simplified approach assumes a single contact surface problem when the flexible strip transfers the applied tension to the spiral surface through the friction effect, gradually increasing the shear stresses on the contact surface.

Fig. 1**a** schematises the spiral anchorage system. The contact surface has no curvature at the entering point, and the CFRP strip direction coincides with the external load **P**. The anchor block fixing hole locates at the same line, preventing the gripping system's rotation and losing the frictional contact. Hence, the fixing reaction has the same magnitude as the force **P**. The curvature of the contact surface gradually increases inward of the spiral support. Therefore, the anchorage system accumulates the shear stresses at the contact surface, steadily reducing the axial force in the CFRP strip. In other words, the frictional forces move the stress concentration inside the anchor, reducing its magnitude.

The previous study [16] showed that the appropriate choice of the spiral surface shape could balance the tension- and bending-induced tensile stresses in the strip remaining below the CFRP tensile strength. The friction coefficient controls the load-transferring process; the contact surface curvature and flexural stiffness define the stress distribution over the strip cross-section height—decreasing the surface curvature decreases the bending stresses but increases the anchorage system's dimensions. This study aims to optimise the anchorage geometry, i.e., to minimise the dimensions of the anchorage block. This limitation is essential for the engineering application of the developed gripping system.

2.3. The analytical model

The model assumes a constant friction coefficient f, absolute rigidity of the spiral support (Fig. 1**a**), inextensible strip material, and rectangular cross-section of the strip. Fig. 1**b** shows the load components acting on the curve segment, where the points O and O_1 are the centres of the curve and the circle of curvature drawn at a point L with radius ρ determined as

$$\rho = ds/d\theta. \tag{1}$$

The following formulas describe the equilibrium condition of the unite curve segment ds in the projection on the n and τ axes (Fig. 1**b**):

$$n: \quad (2\mathbf{P} + d\mathbf{P})\sin\frac{ds}{2\rho} - d\mathbf{N} = 0\,; \tag{2}$$

$$\tau: \quad d\mathbf{P}\cos\frac{ds}{2\rho} - d\mathbf{F}_f = 0, \quad d\mathbf{F}_f = f d\mathbf{N}, \tag{3}$$

where **P**, **N**, and $\mathbf{F}_f$ are the axial, tangential, and frictional forces. The authors [16] expressed the solution of the above equation system in terms of the traction ratio:

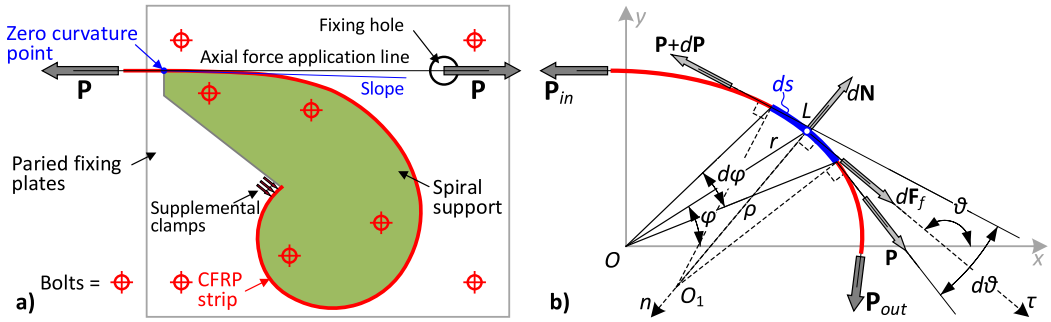

Fig. 1. Spiral frictional anchorage concept: a) a principle scheme; b) force components acting on the flat strip.

$$\chi = \mathbf{P}_{in}/\mathbf{P}_{out} = \exp\left(\int_{\varphi_1}^{\varphi_2} f \bullet \rho^{-1} ds\right), \tag{4a}$$

where $\mathbf{P}_{in}$ and $\mathbf{P}_{out}$ are the load components up-coming to the curve segment ds and out-coming from it (Fig. 1**b**). Under the constant friction coefficient assumption, the above equation transforms as

$$\chi = \exp\left(f \bullet \int_{\varphi_1}^{\varphi_2} \rho^{-1} ds\right). \tag{4b}$$

As mentioned in the previous section, the contact surface curvature affects the dimensions of the anchorage system. The study [16] experimentally investigated the mechanical efficiency of the anchorage block having the logarithmic shape of the CFRP contact surface. Therefore, this study uses this frictional gipping system as the reference; the Archimedean spiral describes the alternative anchorage system because of the potential compactness of the frictional grips. The reader can find a detailed explanation of this choice in the article [16].

The following equations describe the polar coordinate formula and traction coefficients of the logarithmic and Archimedean spirals:

$$r = C_1 \bullet \exp(C_2 \bullet \varphi), \quad \chi = \exp[f \bullet (\varphi_2 - \varphi_1)]; \tag{5}$$

$$r = C_3 \bullet \varphi^n, \quad \chi = \exp\left[f\left(\varphi_2 - \varphi_1 + \tan^{-1}\frac{\varphi_2}{n} - \tan^{-1}\frac{\varphi_1}{n}\right)\right], \tag{6}$$

where C_1, C_2, and C_3 are the geometry coefficients; φ_1 and φ_2 are the initial and final angles of the spiral in polar coordinates, describing the integration boundaries for determining the ratio χ, see equation **(4)**; $n = 1$ is the Archimedean spiral exponent. The above equations demonstrate the importance of the friction coefficient f and the integration bounds on the anchorage efficiency determined by the traction ratio χ.

This study employs the logarithmic spiral coefficients from the article [16]:

$$C_1 = \sqrt{\Phi}; \quad C_2 = \frac{2}{\pi}\ln\sqrt{\Phi}; \quad \Phi = \frac{1+\sqrt{5}}{2}, \tag{7}$$

where Φ is the Golden Ratio. The Archimedean spiral, i.e. Eq. (6), assumes the following coefficient:

$$C_3 = \frac{50}{\pi}. \tag{8}$$

The above coefficient determines the constant distance between the revolution branches equal to 100 mm (under assumption $n = 1$).

The considered anchorage system (Fig. 1**a**) resists the applied tension mainly by frictional forces—the tensile stresses due to the tension and bending loads should not exceed the CFRP strength. The initial radius r_1 depends on the flexural stiffness and strength of the CFRP strip, determining the anchorage joint dimensions. The following equations describe the initial angle of the investigated spirals:

$$\varphi_1 = \frac{\pi}{2} \bullet \left(\frac{\ln r_1}{\ln\sqrt{\Phi}} - 1\right) - \text{logarithmic curve}; \tag{9}$$

$$\varphi_1 = (r_1/C_3)^{1/n} - \text{Archimedian curve}. \tag{10}$$

2.4. The anchorage joint of the pedestrian bridge prototype

This section considers the anchorage joint of the pedestrian bridge prototype tested in the Laboratory of Innovative Building Structures at VILNIUS TECH [7]. The flat ribbons of the bridge prototype faced a 170 kN thrust force. This load is considered the design condition, determining the traction coefficient equal to 56.67 under the assumption that internal mechanical grips (Fig. 1**a**) resist the residual 3 kN axial load. That assumption is acceptable for the bolted fastening joints [23,24]. The CARBOPLATE E 170 by MAPEI is used in this study as the flat ribbon. The producer describes the following material properties: elasticity modulus $E = 170$ GPa; tensile strength $f_u = 3.1$ GPa; thickness $t = 1.4$ mm; width $b = 50$ mm.

Fig. 2**a** and **2b** show the gripping schematics of the logarithmic and Archimedean spirals; the schemes are rotated, distributing the strip horizontally at the anchorage entry. The thick black line shows the CFRP strip. The dashed lines indicate the tangent lines determined at the spiral surface's flat strip entrance and exit. The thin red lines describe the Cartesian coordinates. The Archimedean curve (Fig. 2**b**) determines a more compact anchorage joint than the logarithmic alternative for the same traction ratio χ—the corresponding outer radius r_2 equals 284.5 mm and 586.6 mm.

The previous studies [7,16] identified the strip flexural stiffness as the central feature determining the frictional anchorage geometry because of the axial and bending load summation. In the considered case (rectangular cross-section), the following condition determines the ultimate resistance of the CFRP strip:

$$\frac{\mathbf{P}(\varphi)}{t \bullet b} + E \bullet \frac{t}{2 \bullet r(\varphi)} \le f_u, \quad \varphi \in [\varphi_1; \varphi_2]. \tag{11}$$

The above condition demonstrates that the bending effect increases with increasing the strip thickness t and elasticity modulus E.

Although the Archimedean spiral ensures the compact anchorage joint solution (Fig. 2**b**), it assumes a constant distance between the revolution branches. Still, the frictional stress effect is not identical for each spiral revolution. Tailoring the exponent n in Eqs. **(6) and (10)** can optimise the joint's geometry.

2.5. Optimising the anchorage geometry

The load-bearing capacity of the internal clamps (Fig. 1**a**) determines the required traction ratio:

$$\chi = \mathbf{P}/\mathbf{R}, \tag{12}$$

where $\mathbf{P}$ and $\mathbf{R}$ are the applied load and resistance of the internal clamps (Fig. 1**a**). The following equation accounts for the bending effect, describing the inner radius r_1 under the assumption of $\mathbf{P}(\varphi) = \mathbf{R}$:

$$r(\varphi) = 10 \bullet \left\| \gamma \bullet E \frac{t}{2 \cdot (f_u - \mathbf{P}(\varphi)/t \bullet b)} \bullet 0.1 + 0.5 \right\|, \tag{13}$$

where γ is the safety factor (in the study [16], $\gamma = 1.5$ was used following the authors' engineering judgement); the norm $\|x\|$ defines the rounding of the operand x to the nearest integer number. The above expression ensures rounding the required radius up to 10 mm. Eq. **(10)** determines the corresponding angle φ_1.

The following formula defines the iterative solution process because of the emergence of the unknown angle φ_2 in both equation sides:

$$\varphi_2 = \tan^{-1}\frac{\varphi_1}{n} - \tan^{-1}\frac{\varphi_2}{n} + \frac{\ln\chi}{f} + \varphi_1, \tag{14}$$

where f is the friction coefficient; this study employs the experimental value of this coefficient, which was determined on the cylindrical surface and verified through the theoretical analysis in the article [16], i.e. $f = 0.4$. The assumed value also corresponds to the friction parameter reported by Katsumata et al. [25].

Eq. **(13)** defines the required outer radius r_2 by assuming $\mathbf{P}(\varphi) = \mathbf{P}$. The following expression finalises the optimisation process, determining the efficient exponent of the power function in formula **(6)**:

$$n = \ln\left(\frac{r_2}{C_3}\right)/\ln\varphi_2. \tag{15}$$

The article [26] describes the possible iterative solution using Excel spreadsheets.

Fig. 2**c and 2d** show the Archimedean spiral's optimisation examples. Fig. 2**c** represents the solution alternative to Fig. 2**b**. The proposed

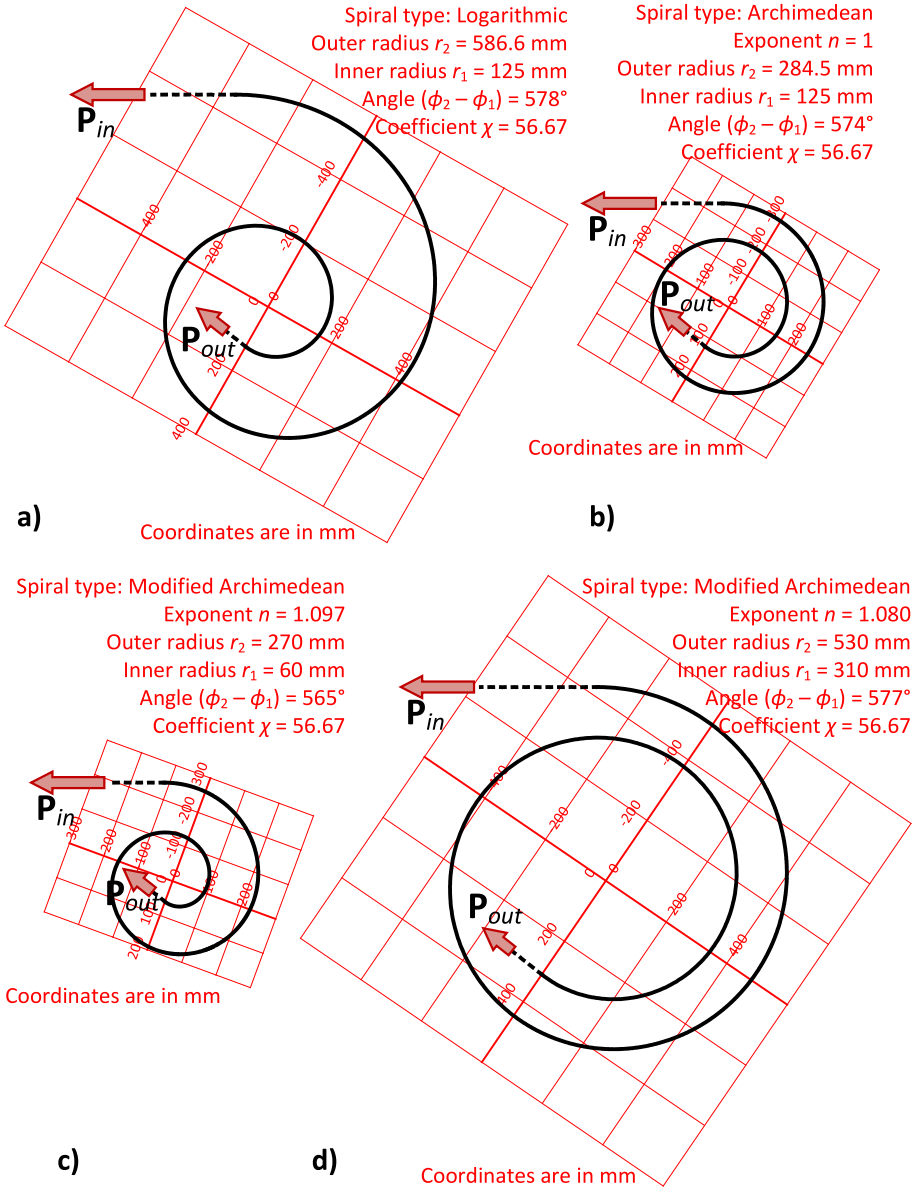

Fig. 2. Stress-ribbon bridge anchorage joints: a) logarithmic spiral for 1.4 mm thickness strip; b) Archimedean spiral for 1.4 mm strip; c) and d) the Archimedean spirals optimised for 1.4 mm and 4 mm CFRP strips.

optimisation process reduces the inner and outer radii from 125 mm and 284.5 mm to 60 mm and 270 mm, though the geometry does not change substantially.

Fig. 2**d** shows the results determined for the CFRP strip with the following geometry and mechanical properties: elasticity modulus E = 200 GPa; tensile strength f_{tl} = 2.0 GPa; thickness t = 4 mm; width b = 50 mm. The comparison of Fig. 2**c** and **2d** reveals that the strip properties affect the frictional anchor geometry designed for the same conditions, i.e. the geometry coefficient $C_3 = 50/\pi$, the load $\mathbf{P}$ = 170 kN, the traction coefficient χ = 56.67, and the safety factor γ = 1.5. Notwithstanding the increase in the load-bearing capacity of the alternative strip (2.0 × 4 × 50 = 400 kN > 3.1 × 1.4 × 50 = 217 kN), the CFRP parameters' alteration increases the inner and outer radii from 60 mm and 270 mm to 310 mm and 530 mm, i.e. more than two times.

3. Experimental verification of the model

This section experimentally verifies the adequacy of the theoretical assumptions (**Section 2.3**), the design constraints expressed in the traction coefficient, χ, and the safety factor, γ, terms, and the optimisation procedure itself (**Section 2.5**). This verification extends the experimental approach from the article [16] and, thus, addresses the results of the already tested logarithmic spiraloid. Thus, the following section briefly summarises the published outcomes.

3.1. Logarithmic anchorage system

The study [16] developed the logarithmic spiral prototype from polylactic acid (PLA) using 3D printing technology. The test object was the 10 × 0.5 × 1000 mm CFRP strip specimens from Easy Composites (UK). The mechanical tests of the CFRP samples and preliminary analytical calculations, Eq. **(11)**, determined the allowable initial radius r_1 = 60 mm; Eqs. **(9) and (10)** have defined the initial angle φ_1 of the logarithmic spiral as 25.16 rad. Fig. 3**a** shows the corresponding schematic determined for the 2π angle of the contact surface.

Fig. 3**b** shows the tested polymeric prototype of the logarithmic frictional grips. The additional conical grips were located inside the anchorage system to activate the friction forces during the initial loading

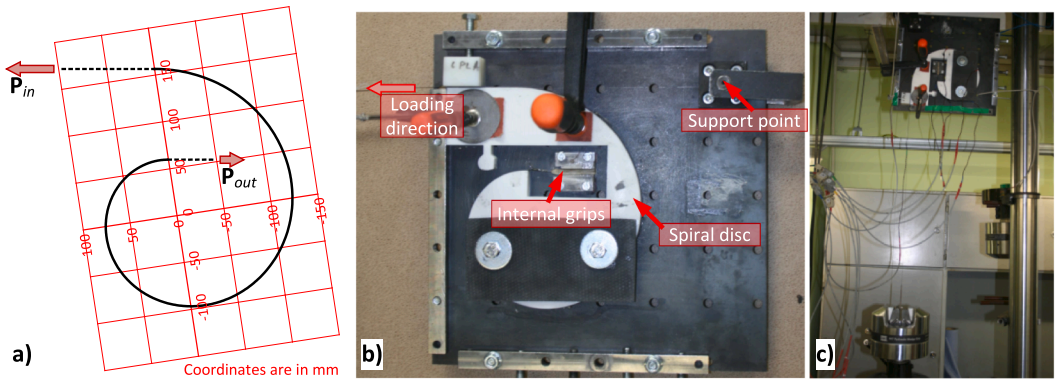

Fig. 3. Anchorage prototype tested in [16]: a) logarithmic spiral; b) the polymeric prototype; c) tests setup.

stage. Fig. 3**c** demonstrates the test setup. Fig. 3**a** describes the geometry of the frictional surface.

The tests [16] proved the proposed gripping system efficiency—the CFRP strip failure (localised outside the anchorage block) has resulted from the tensile stresses exceeding the CFRP strength. The tests also proved the analytical model described in **Section 2.3**—the average coefficient χ was equal to 12.2, which agrees with the theoretically predicted value of 12.5 from Eq. **(5)**.

3.2. Optimised Archimedean prototypes

The test setup, materials, and prototyping technology in this study are identical to the investigation [16] except for the pultruded CFRP strips purchased from the same manufacturer (Easy Composites) but after two years from the first tests. Similarly to the previous study, the 300 mm long coupons of the 0.5 × 10 mm CFRP strip were tested following the ASTM D 3039/D 3039 M−07 standard requirements. The following characteristics were obtained in the tension tests: ultimate stress $\sigma_{x,u}$ = 1695.1 ± 20 MPa, ultimate strain $\varepsilon_{x,u}$ = 1.08 ± 0.04%, and elastic modulus E_x = 149.1 ± 3.1 GPa. In the previous tests [16], the corresponding values were 1897.7 ± 49 MPa, 1.27 ± 0.04%, and 138.2 ± 0.9 GPa. The 10% reduction in the tensile strength of the CFRP material is noticeable.

Two alternative gripping systems were designed using the modified Archimedean spiral as governing curve, i.e. Eq. **(10)**. **Section 2.5** describes the prototype geometry determination procedure; Table 1 provides the design parameters. The mechanical parameters of the CFRP strip were assumed from the tests [16]. The previous investigation used the safety coefficient value typical for structural applications [6,23], i.e. 1.5; the mechanical performance of the 3D-printed polymeric material was also unknown. However, the physical tests [16] demonstrated outstanding performance of the printed grips and the efficiency of the frictional anchorage system (ensuring the necessary traction ratio) and sufficient treatment quality of the frictional contact surface, avoiding the stress concentration in the CFRP strip.

The above result ensured the safety factor reduction to 1.15 in this work, reducing the anchors' geometric dimensions (radius) for 3D printing. The current physical experiments will check the adequacy of this assumption. Note that the safety factor affects only the local stress concentration because of the combined action of the axial force and bending moment [Eq. **(13)**] and does not affect the traction ratio, representing the design object. In other words, the frictional surface quality characteristics define the assumed safety parameter. At the same time, extensive tests are necessary to determine the adequate safety factor value for developing the frictional gripping device. Furthermore, the cyclic loads, typical for bridge superstructures [4,7], could affect the anchors' mechanical resistance.

Table 1
Design parameters of the modified Archimedean spirals.

Parameter	Spiral S10	Spiral S20
Design load, **P** [kN]	8	8
Traction coefficient, χ	10	20
Friction coefficient, f	0.4	0.4
Safety factor, γ	1.15	1.15
CFRP strip geometry width × thickness [mm]	10 × 0.5	10 × 0.5
CFRP strength, f_u [MPa]*	1900	1900
CFRP modulus of elasticity, E_f [GPa]	140	140

* The value from the previous tests [16].

Table 1 indicates that only the traction coefficient was the design variable in this study, and the specimen notation highlight this fact. Fig. 4 shows the designed spirals and corresponding models adopted for 3D printing. The developed models include space for the internal grips.

This study employs the same equipment and printing procedure as the research [16]. Furthermore, the authors experimentally determined the mechanical characteristics of the printed material, polylactic acid (PLA), in the study [27]. The tests identified the following material parameters: the tensile strength = 37.7 MPa and the elastic modulus = 5.8 GPa. The 3D models of the spiral disks (Fig. 4) were created with AutoCad and processed using PrusaSlicer 2.3.3 software. The printing layout contained 50 layers of 0.3 mm in height. The 15 mm thickness anchorage prototypes were produced using a Prusa i3 MK3 3D printer with the following printing parameters: the speed = 40 mm/s; the volumetric flow rate = 5 mm^3/s; the extrusion nozzle and printing bed temperatures were equal to 215 °C and 60 °C. The identical printing layout of both prototypes assumed two "shells" having 100% infill, which formed the perimeter surfaces of the prototypes; the rectilinear raster infill created the sample body having 60% density.

The previous study [16] estimated the friction coefficient, f, on the cylindrical surface with sandpaper #800 as 0.40 ± 0.03 (mean value from five tests). Therefore, before the mechanical tests, the sandpaper was adhesively connected to the surface in contact with the CFRP strip. This procedure ensured the spiral disc's exact (known) friction characteristics—this condition is mandatory for the analytical model (**Section 2.3**). In addition, the sandpaper smoothed the 3D printing defects (grooves of the printing layers), avoiding local failure of the unidirectional CFRP strip. After that, the printed disks were mounted on the steel support plate using 6 mm bolts and centred in the test apparatus, as Fig. 5 shows.

Test results of six 1000 mm long CFRP samples (three specimens for each spiral anchor, Fig. 4) define the object of this study. The MTS 809.40 servo-hydraulic testing apparatus (MTS Systems Corp., USA) with 250 kN load cell applied the external tension under displacement control and 2 mm/min speed. Fig. 5**b** and **5c** show the test setup. The previous tests [16] identified unstable deformation behaviour of CFRP strip corresponding to the initial, small deformation range because of the finite slippage of the internal grips (Fig. 3**b**). On the other hand, the strain measurements [16] did not identify significant deformations localised

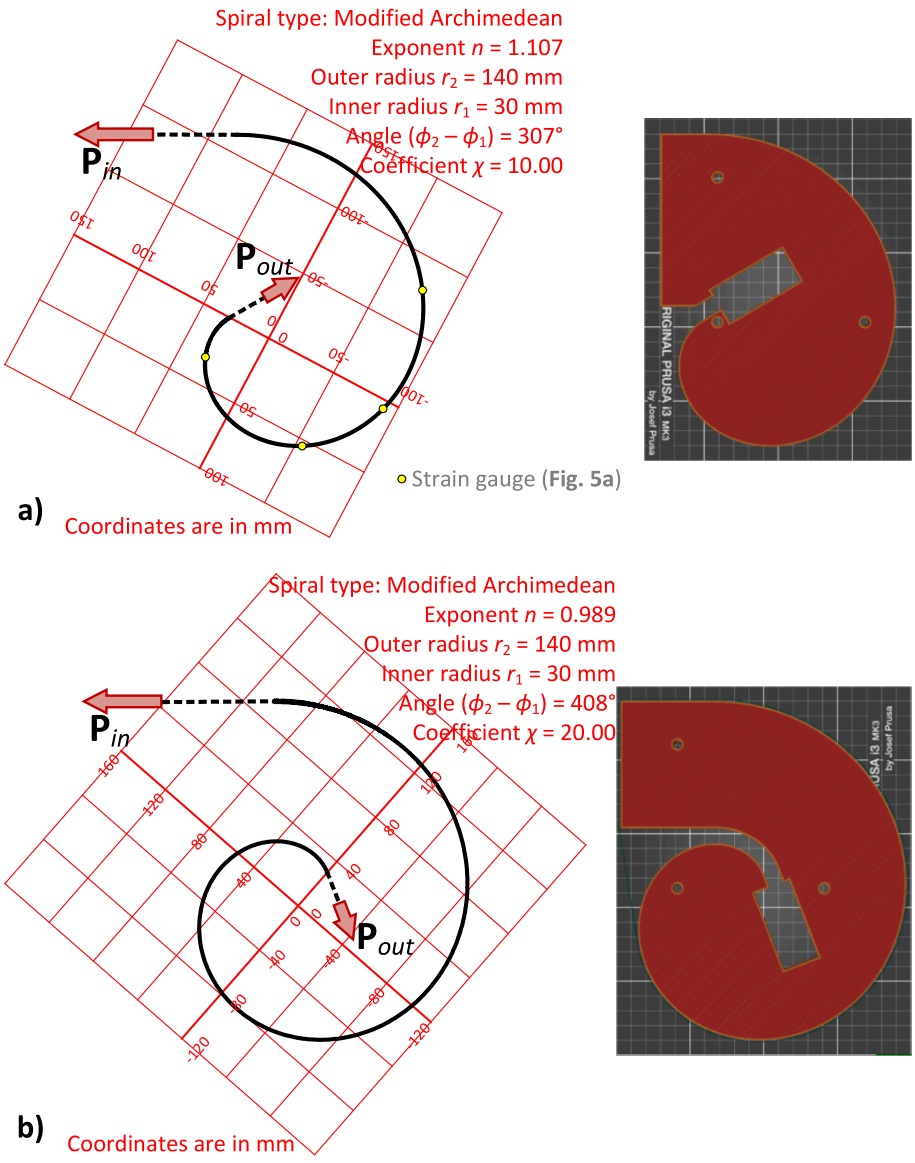

Fig. 4. Modified Archimedean anchorage schematics and corresponding models for 3D printing: a) spiralod S10; b) spiraloid S20.

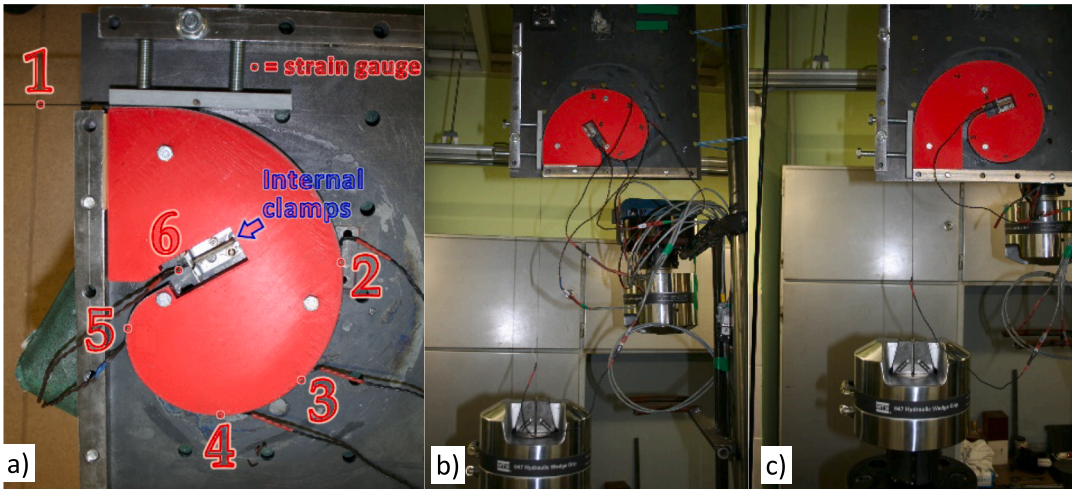

Fig. 5. Modified Archimedean anchorage: a) internal fixator of the CFRP strip (numbers indicate the stain-gauge position); b) test setup S10; c) test setup S20.

near the extra grips. For instance, the minimal traction coefficient indicates a decuple reduction of the design load (=8 kN). Therefore, this study employs the simplified supplemental gripping system, where a grooved steel angle replaced the conical grips. Fig. 5**a** shows a close view of the internal clamps. All specimens in this study were pre-loaded up to 2 kN to tighten the test components and activate the internal fixator. After that, the external loading was diminished until the zero reaction, but minimal tension remained on the strip; the indicators (strain gauges) were zeroed, and the test went forward to failure of the CFRP specimen.

3.3. Test results of the Archimedean prototypes

Six 120 Ω strain gauges with a 1.5 mm measurement base measured deformations of the CFRP strip, as Fig. 5**a** shows—the devices "1″ and "6" were placed at the straight segments of the CFRP strip outside and inside the spiral grips; four remaining gauges were distributed over the contact surface. The latter readings estimated the bending effect simulated by the second component of the sum in Eq. (11), where the fraction describes the bending-induced tension strain $\varepsilon(\varphi)$ in the CFRP strip of thickness t. Following this approach and projecting the gauge location to the printing scheme (Fig. 4**a**), the local radii $r_2 = 88$ mm, $r_3 = 75$ mm, $r_4 = 56$ mm, and $r_5 = 37$ mm would induce the following strains in the CFRP strip ($t = 0.5$ mm): $\varepsilon_2 = 0.284\%$, $\varepsilon_3 = 0.333\%$, $\varepsilon_4 = 0.446\%$, and $\varepsilon_5 = 0.676\%$. These theoretical strain values agree well with the bending deformations of the strip measured at fully assembled spiraloid S10 before the mechanical loading, i.e. $\varepsilon_2 = 0.289\%$, $\varepsilon_3 = 0.332\%$, $\varepsilon_4 = 0.447\%$, and $\varepsilon_5 = 0.684\%$, proving the theoretical concept in **Section 2.3**.

Fig. 6**a** shows the CFRP strip deformations measured on a tested S10 anchor related to the external load **P**. Three identical spiral anchors were tested to ensure the reliability of the results. The strip failure outside the gripping system resulted from all these tests. This outcome proves the reliability of the proposed anchorage concept. In particular, the tests demonstrated the 8.59 kN, 8.57 kN, and 8.87 kN ultimate resistance of the CFRP strip (i.e. 8.68 ± 0.17 kN) that agree with the tensile coupon resistance (8.27 ± 0.16 kN) determined following the ASTM D 3039/D 3039 M−07 standard requirements (**Section 3.2**).

Remarkably, Fig. 6**a** demonstrates the deformation diagrams neglecting the bending effect on the stress-ribbon deformation state, i.e. the "2″-"5" gauges' readings captured before the mechanical loading. Such representation of the test results is typical for field measurements, e.g., [5,13]. However, the previous study [16] highlighted the essential bending effect on the mechanical resistance of flat CFRP composites. Therefore, Fig. 6**b** shows the deformation diagrams shifted to the position corresponding to the initial strains measured at the outer surface of the CFRP strip (Fig. 5**a**).

As expected, the ultimate deformation of the shifted diagrams does not reach the maximum value estimated by the gauge "1″ (placed outside the anchorage system) that well agrees with the ultimate strain $\varepsilon_{x,u} = 1.08 \pm 0.04\%$ defined in the standard tests (Fig. 6**b**). Fig. 6**a** shows the overlapping of the diagrams corresponding to the "5" and "6" gauges' readings; Fig. 6**b** demonstrates the mirrored inclination change of these diagrams corresponding to the 5 kN load. All S10 anchorage samples showed almost identical deformation behaviour. Such an outcome could indicate a minor release of deformations between the "5" and "6" gauges, resulting from insufficient length of the frictional contact surface and inefficient location of the fixing hole near the inner edge weakening the polymeric support (Fig. 4**a**).

The above limitations were considered when composing an alternative spiraloid, where the traction factor was doubled. The alternative S20 gripping system was equipped only with two strain gauges ("1″ and "6") to simplify the testing layout (Fig. 5**c**).

The S20 anchor set consisted of three identical samples of CFRP strip in the same manner as the S10 series. None of the tested samples faced failure of the CFRP strip inside the gripping spiral system. Unfortunately, only one CFRP sample reached the expected ultimate load (8.70 kN); Fig. 7**a** shows the deformation diagrams of the tested S20 anchor. The explanation for the premature failure of the other two samples (the maximum load was equal to 6.48 kN and 6.10 kN) could be related to the production technology—the latter two CFRP samples belonged to the newest batch of the same producer and were purchased after two years from the first specimen series considered in all the previous tests and demonstrated the ultimate resistance exceeding 8 kN.

4. Discussion of the test results

4.1. Adequacy of the theoretical model

Fig. 7**b** shows the traction coefficients for the tested spiral anchorage prototypes. The vertical dashed lines on the diagram indicate the theoretical values of this coefficient. A good agreement between the predicted and actual traction coefficient values can be observed in a specific loading range. The model demonstrates the 6.1% and 6.4% prediction errors for the S10 and S20 anchors in the shaded areas. These results align with the previous tests of the logarithmic spiral, where prediction error did not exceed 3% (**Section 3.1**).

A minor release of deformations between the "5″ and "6" gauges discussed in **Section 3.3** explains the sudden decrease of the coefficient χ in the S10 sample below the target value (=10). On the other hand, the variation of the friction coefficient explains the prediction inadequacy corresponding to the relatively small loading magnitudes. The latter effect could also result from the pre-loading procedure (**Section 3.2**)—the diagrams in Fig. 7**b** stabilise after the pre-loading bound (≈ 2 kN). However, this issue requires further investigation.

The shaded areas in Fig. 7**b** cover the serviceability loading range of the stress-ribbon structures, which typically corresponds to 55%-60% of the ultimate load [7]. In the considered case, the 5.0 ± 0.2 kN load determines the service condition. Therefore, the above results prove the

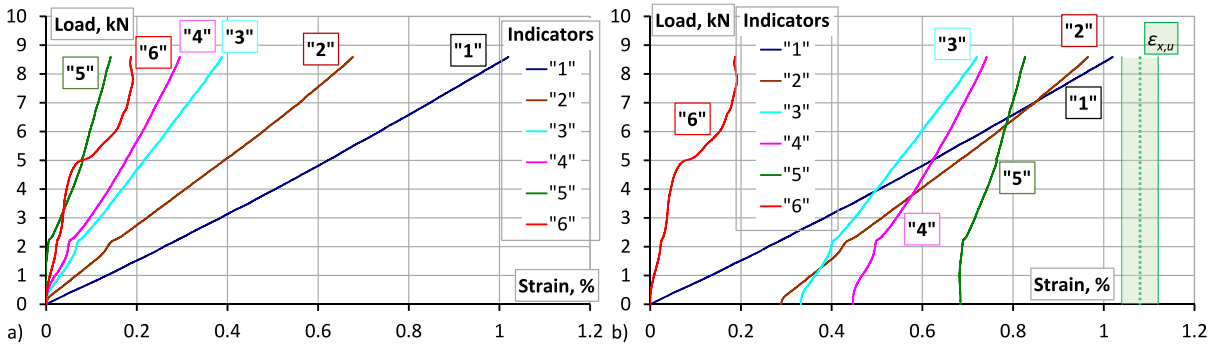

Fig. 6. CFRP strip deformations measured on spiraloid S10 (Fig. 5**a** specifies of the strain gauge notation): a) experimental measurements; b) shifted diagrams accounting for the bending effect ($\varepsilon_2 = 0.289\%$, $\varepsilon_3 = 0.332\%$, $\varepsilon_4 = 0.447\%$, and $\varepsilon_5 = 0.684\%$).

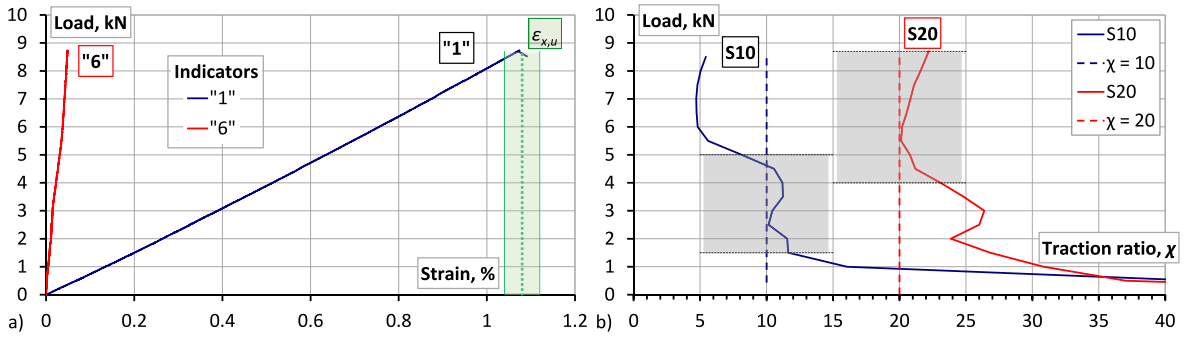

Fig. 7. Spiraloid tests: a) measured CFRP strip deformations on sample S20; b) traction ratios.

adequacy of the simplified theoretical model (Section 2.5) for the design of the spiral anchors of the stress-ribbon structural system employing high-strength CFRP flat strips, as Fig. 2 exemplifies.

The proposed design equations (Section 2.5) allow compact distribution of the spiral evolutions by satisfying the local strength condition of the composite strip, Eq. (13). The spiral schematics in Fig. 4 show the characteristic examples when only the strength condition determines the dimensions of the spiral grips. In other words, both anchors have identical internal and external radii, r_1 and r_2, which depend on the strip strength and stiffness, but ensure different traction ratios, χ, distributing different curvature lengths within the $[r_1; r_2]$ dimension interval.

The slope of the diagrams "2″-"5" (Fig. 6) is dependent on the distance of strain gauges to the strip entrance to the gripping device. This deformation behaviour is associated with the friction force cumulative nature, reducing deformations of the strip—the decrease in the strains decreases the curve slope. Moreover, none of the modified diagrams (Fig. 6**b**) reaches the CFRP strip ultimate deformation (1.08 ± 0.04%, Section 3.2). On the one hand, that proves the correctness of the choice of the curved shape of the anchorage block (Fig. 4**a**). On the other hand, the consistency of the mechanical parameters of the CFRP strip obtained during the standard and spiraloid tests proves the suitability of the proposed frictional anchorage system for physical testing purposes.

4.2. Future research

The previous study [16] revealed the marginal importance of the deformability of the spiral support on the deformation prediction of the CFRP strip inside the grips. On the contrary, the variable friction coefficient significantly alters the deformation behaviour of the strip. Fig. 7**b** shows the considerable disagreement between the theoretical model and experimental results. In other words, the Eq. (4a) transformation to formula (4b) is allowable with significant reservation, and future research should investigate the friction coefficient evolution corresponding to the small deformations range.

Notwithstanding the above reservation, the adequacy of the proposed design procedure (Section 2.5) is acceptable for developing efficient stress-ribbon structures. Furthermore, the computer-based additive manufacturing principles fit Industry 4.0, accelerating its development [28]. However, the prototypes can inadequately replicate the mechanical resistance of physical objects [29]. Therefore, the upcoming studies should implement the proposed prototyping technique (Section 3.1) to develop full-scale stress-ribbon structures, e.g., investigated in the article [7] and depicted in Fig. 2**c** and **2d**. In this context, the effects of dynamic loads, characteristic of slender stress-ribbon systems, determine the object for future research. In addition, the references [5,7] pointed out the positive effect of the ribbon pre-stress for solving the slenderness problem. Therefore, this technique defines a promising modification of the proposed frictional anchorage system.

5. Conclusions

This manuscript describes an innovative concept for designing a frictional anchorage system for flat CFRP strips suitable for developing stress-ribbon structural systems. The proposed spiral anchor resists the applied tension mainly by frictional forces: the balance between the support curvature's increase and the tension force's decrease controls the tension stresses in the strip. This manuscript proposes the corresponding design procedure for frictional spiral anchorage systems; the experimental verification substantiates the modelling results. The following significant conclusions come from this study:

- The proposed iterative design procedure minimises the gripping system size, satisfying the CFRP strength limitation when the developed modified Archimedean spiral determines the shape of the spiral contact surface. For example, the proposed modification reduced the size of the frictional support two times regarding the logarithmic spiral considered in the previous study. Therefore, this modification allows the practical application of the proposed methodology for designing stress-ribbon structural systems employing high-strength flexible CFRP strips.
- The experimental verification of the proposed theoretical concept demonstrates acceptable adequacy of the CFRP strip deformation predictions—the prediction error of the ratio between the external and outcome loads does not exceed 7%. The adequate predictions cover the service loading range of the stress-ribbon systems. In addition, increasing the frictional contact length improves (stabilises) the mechanical resistance of the anchorage join.
- The friction coefficient variation corresponding to relatively small deformations and the frictional anchor resistance to dynamic loads determine the further research object.

CRediT authorship contribution statement

Viktor Gribniak: Methodology, Supervision, Resources, Validation, Formal analysis, Visualization. **Aleksandr K. Arnautov:** Conceptualization, Investigation, Formal analysis, Data curation, Validation. **Arvydas Rimkus:** Visualization, Software, Project administration.

Declaration of Competing Interest

The authors declare that they have no known competing financial interests or personal relationships that could have appeared to influence the work reported in this paper.

Data availability

The raw/processed data required to reproduce these findings cannot be shared as the data also forms part of an ongoing study.

Acknowledgement

The authors acknowledged financial support from European Regional Development Fund (Project No 01.2.2-LMT-K-718-03-0010) under a grant agreement with the Research Council of Lithuania (LMTLT).

References

[1] Gribniak V. Special Issue "Advanced Composites: From Materials Characterization to Structural Application". Materials 2020;13(24), Paper ID: 5820; https://doi.org/10.3390/ma13245820.
[2] Vuković NK, Jevrić M, Zejak R. Experimental analysis of RC elements strengthened with CFRP strips. Mech Compos Mater 2020;56(1):75–84. https://doi.org/10.1007/s11029-020-09861-x.
[3] Hong H, Bae KJ, Jung H, Oh Y, You N-H, Lee J-C, et al. Preparation and characterization of carbon fiber reinforced plastics (CFRPs) incorporating through-plane-stitched carbon fibers. Compos Struct 2022;284:115198. https://doi.org/10.1016/j.compstruct.2022.115198.
[4] Liu Y, Gu M, Liu X, Tafsirojjaman T. Life-cycle cost analysis of long-span CFRP cable-stayed bridges. Polymers 2022;14, Paper ID: 1740. https://doi.org/10.3390/polym14091740.
[5] Arnautov AK, Kulakov V, Andersons J, Gribniak V, Juozapaitis A. Experimental investigation on stiffness and strength of single-lap z-pinned joints in a laminated CFRP stress-ribbon strip. The Baltic Journal of Road and Bridge Engineering 2016;11(2):120–6. https://doi.org/10.3846/bjrbe.2016.14.
[6] Matsuo T, Hojo M, Kageyama K. Influence of gripping method on tensile properties of unidirectional thermoplastic CFRP–Round-robin activity for international standardization in Japan. J Compos Mater 2019;53(28–30):4161–71. https://doi.org/10.1177/0021998319855419.
[7] Juozapaitis A, Sandovič G, Jakubovskis R, Gribniak V. Effects of flexural stiffness on deformation behaviour of steel and FRP stress-ribbon bridges. Applied Sciences 2021;11(6), Paper ID: 2585; https://doi.org/10.3390/app11062585.
[8] Portnov GG, Kulakov VL, Arnautov AK. Grips for the transmission of tensile loads to a FRP strip. Mech Compos Mater 2013;49(5):557–74. https://doi.org/10.1007/s11029-013-9363-1.
[9] Heydarinouri H, Vidovic A, Nussbaumer A, Ghafoori E. FE analysis and experimental validation of mechanical wedge–barrel anchors for CFRP rods. Compos Struct 2021;275:114509. https://doi.org/10.1016/j.compstruct.2021.114509.
[10] Wang X, Xu P, Wu Z, Shi J. A novel anchor method for multitendon FRP cable: manufacturing and experimental study. J Compos Constr 2015;19(6):04015010. https://doi.org/10.1061/(ASCE)CC.1943-5614.0000563.
[11] Zhu W, Wei W, Liu F, Zeng R. Method of designing a friction-based wedge anchorage system for high-strength CFRP plates. Materials 2021;14, Paper ID: 6443; https://doi.org/10.3390/ma14216443.
[12] Ai P, Feng P, Lin H, Zhu P, Ding G. Novel self-anchored CFRP cable system: Concept and anchorage behaviour. Composite Structures 2021;263, Paper ID: 113736; https://doi.org/10.1016/j.compstruct.2021.113736.
[13] Schlaich M, Bleicher A. Carbon fibre stress-ribbon bridge. Bautechnik 2007;84(5):311–9. https://doi.org/10.1002/bate.200710028 (in German).
[14] Liu Y, Zwingmann B, Schlaich M. Carbon fiber reinforced polymer for cable structures—A review. Polymers 2015;7:2078–99. https://doi.org/10.3390/polym7101501.
[15] Meier U, Winistoerfer A. Multilayer Traction Element in the Form of a Loop, US-Patent 6,209,279 B1, 2001.
[16] Gribniak V, Arnautov AK, Rimkus A. The development of nature-inspired gripping system of a flat CFRP strip for stress-ribbon structural layout. J Comput Des Eng 2021;8(2):788–98. https://doi.org/10.1093/jcde/qwab014.
[17] Hart-Smith LJ. (1980). Mechanically fastened joints for advanced composites–Phenomenological considerations and simple analyses. In Lenoe EM et al. (Eds.) Fibrous composites in structural design. Plenum Press, NY. 1980, pp. 543-574.
[18] Tahir MM, Wang W-X, Matsubara T. A novel tab for tensile testing of unidirectional thermoplastic composites. J Thermoplast Compos Mater 2019;32(1):37–51. https://doi.org/10.1177/0892705717743295.
[19] Portnov GG, Kulakov VL, Arnautov AK. A refined stress-strain analysis in the load transfer zone of flat specimens of high-strength unidirectional composites in uniaxial tension 1. Theoretical analysis. Mech Compos Mater 2006;42(6):547–54. https://doi.org/10.1007/s11029-006-0065-9.
[20] Ye H, Zhang Q, Liu C, Wu C, Duan Z. Failure mechanisms governing anchoring force of friction-based wedge anchorage for prestressed CFRP plate. Compos Struct 2019;225:111142. https://doi.org/10.1016/j.compstruct.2019.111142.
[21] Pagano F, Paulmier P, Kaminski M, Thionnet A. Numerical and experimental approach for improving quasi-static and fatigue testing of a unidirectional CFRP composite laminate. Procedia Eng 2018;213:804–15. https://doi.org/10.1016/j.proeng.2018.02.076.
[22] Eliasson S, Wanner S, Barsoum Z, Wennhage P. Development of fatigue testing procedure for unidirectional carbon fiber composites. Procedia Struct Integrity 2019;19:81–9. https://doi.org/10.1016/j.prostr.2019.12.010.
[23] Mohee FM, Al-Mayah A, Plumtree A. Anchors for CFRP plates: State-of-the-art review and future potential. Compos B Eng 2016;90:432–42. https://doi.org/10.1016/j.compositesb.2016.01.011.
[24] Zhu Y, Zhu H, Gribniak V. Analyzing the sample geometry effect on mechanical performance of drilled GFRP connections. Materials 2022;15, Paper ID: 2901; https://doi.org/10.3390/ma15082901.
[25] Katsumata T, Mizutani Y, Todoroki A, Matsuzaki R. A fundamental study on static strength improvement of CFRP bolted joints by increasing friction force. J Solid Mech Mater Eng 2010;4(6):711–9. https://doi.org/10.1299/jmmp.4.711.
[26] Kaklauskas G, Gribniak V. Hybrid tension stiffening approach for decoupling shrinkage effect in cracked reinforced concrete members. J Eng Mech 2016;142(11):04016085. https://doi.org/10.1061/(ASCE)EM.1943-7889.0001148.
[27] Shkundalova O, Rimkus A, Gribniak V. Structural application of 3D printing technologies: mechanical properties of printed polymeric materials. Sci–Future of Lithuania 2018;10, Paper ID: mla.2018.6250; https://doi.org/10.3846/mla.2018.6250.
[28] Ceruti A, Marzocca P, Liverani A, Bil, C. Maintenance in aeronautics in an Industry 4.0 context: The role of Augmented Reality and Additive Manufacturing. J Comput Des Eng 2019;6:516–26; https://doi.org/10.1016/j.jcde.2019.02.001.
[29] Althammer F, Ruf F, Middendorf P. Size optimization methods to approximate equivalent mechanical behaviour in thermoplastics. J Comput Des Eng 2021;8(1):170–88. https://doi.org/10.1093/jcde/qwaa069.